Indian Journal of Pure & Applied Physics
Vol. 62, April 2024, pp. 320-328
DOI: 10.56042/ijpap.v62i4.5661

Investigation of Photocatalytic and Photoluminescent Properties of a Novel Multifunctional Near-UV Excited NanoStucture CeO_2:0.1Dy0.1Ho

Handan Özlü Torun[a]*, Esra Öztürk[b] & Rabia Kırkgeçit[c]

[a]Department of Energy System Engineering, Kahramanmaraş İstiklal University, Kahramanmaraş 46300, Turkey

[b]Department of Metallurgical and Materials Engineering, Karamanoglu Mehmetbey University, Karaman 70100, Turkey

[c]Institute of Science, Material Science and Engineering, Kahramanmaraş Sütçü İmam University, Kahramanmaraş, 46050, Turkey

Received 18 September 2023; accepted 22 January 2024

In this study, Dy^{3+} doped and Ho^{3+} co-doped materials synthesized by the sol-gel method at different temperatures were investigated. The structural and optical properties were characterized by an x-ray powder diffract meter, thermal analysis system, scanning electron microscopy, Raman spectroscopy, FT-IR, UV-vis spectroscopy, and photoluminescence spectrophotometer. The photocatalytic performance, crucially contingent on the sintering temperature, was systematically evaluated using malachite green and methylene blue as model pollutants. Remarkably, the highest efficiency, registering an impressive 90%, was achieved for methylene blue when sintered at 1000 °C. For malachite green, a substantial efficiency of 62% was attained at a sintering temperature of 800 °C. The corresponding optical band gap, a pivotal parameter influencing photocatalytic activity, was determined to be 2.43 eV. Under the near-UV excitation at 318 nm, the CeO_2:0.1Dy0.1Ho phosphor emitted photoluminescence with dominating emissions at 475 nm (blue), 559 nm (green) and 663 nm (red) corresponding to $^4F_{9/2}\rightarrow{}^6H_{15/2}$ (blue) transition of Dy^{3+} ions, $^5F_4,{}^5S_2\rightarrow{}^5I_8$ (green) and $^5F_5\rightarrow{}^5I_8$ (red) transitions of Ho^{3+} ions, respectively.

Keywords: CeO_2; Photocatalytic; Photoluminescence

1 Introduction

CeO_2 is a metal oxide compound in the lanthanide group. CeO_2 and its compounds, which have cubic fluorite structure, chemical stability and wide band gap, have become widespread in many fields in recent years[1-3]. Multifunctional CeO_2 contains a high amount of oxygen vacancies in its crystal structure due to the Ce^{4+}/Ce^{3+} reduction reaction. These formed oxygen vacancies allow CeO_2 to be used as a ceramic electrolyte as well as having a photocatalytic effect[4-7]. At the same time, the 4f orbitals display luminescent properties, making them useful in optoelectronic devices[7-9]. So far, the luminescence[10-15] and photocatalytic[16-20] behaviors of CeO_2 compounds formed with the contribution of some lanthanide group elements have been examined.

Luminescence materials with blue, green and red emission are extremely important for w-LEDs[21-23]. At this point, trivalent dysprosium (Dy^{3+}) ion comes to the fore and is intensively researched due to its blue and green emissions. The predominance of blue emission (~484 nm, $^4F_{9/2}$–$^6H_{15/2}$) or yellow emission (~575 nm, $^4F_{9/2}$–$^6H_{13/2}$) of Dy^{3+} ions varies within different host crystals. The yellow emission of Dy^{3+} ions is highly influenced by the chemical environment of Dy^{3+}, while the blue emission is relatively more stable[24]. Up to now, there are many host crystals that can be activated by Dy^{3+} ions[25-29].

On the other hand, it is well known that the photocatalytic properties of CeO_2 can be significantly improved by substituting rare earth ions for Ce^{4+} in the crystal lattice. Because of donor or acceptor levels between the valence and conduction bands by the doped ions, the electrons and holes are produced to increase the photoactivity[30].

When previous studies are examined, the reports of photocatalyst and photoluminescence studies of rare earth ion pair doped CeO_2 compounds are quite limited. The research aims to increase the dye removal percentage under visible light by using photocatalyst compounds of dyestuffs that cause environmental pollution and to obtain radiation in the visible region in optoelectronic devices[31,32]. In addition, in this study, the photochemical (luminescence/photocatalysis) properties of the CeO_2:0.1Dy0.1Ho compound formed by doping (Dy, Ho) pair were examined for the first time, depending on the sintering temperature.

*Corresponding author: (E-mail: handan.ozlutorun@istiklal.edu.tr)

1 Material and Methods

2.1 Material synthesis

Sol-gel method was used in the synthesis process of CeO_2:0.1Dy0.1Ho compound. Starting compounds cerium (III) nitrate hexahydrate [Ce(NO3)3.6H2O] (purity 99.99%, Alpha Aesar), holmium(III) nitrate pentahydrate [Ho(NO3)3.5H2O] (purity 99.9%, Arcos organics)) and dysprosium (III)nitrate hexahydrate [Dy(NO3)3.6H2O] (purity 99.9%, Arcos organics) were weighed in 0.1 mmol proportions. These compounds were dissolved in 25 ml of pure water. 25 mmol of citric acid (Sigma-Aldrich 99.9%) and 8 mmol of ethylene glycol (Sigma-Aldrich 99.9%) were added to the solution. The solution was heated until gelation occurred. After gelation, pre-drying was done. The dark brown sample was sintered at 600, 800 and 1000 °C for 18 hours, respectively. The synthesis steps are summarized in Fig. 1.

2.2 Forbidden band gap measurement

First of all, 10 mg of the powder sample with CeO_2:0.1Dy0.1Ho was weighed on a sensitive digital precision balance. The weighed sample was placed in a glass tube. Approximately 10 ml of ethyl alcohol was added to the sample. Ethyl alcohol aqueous solutions were mixed in an ultrasonic water bath for approximately 2 minutes. After the process was completed, measurements were taken using a UV-spectrophotometer (UV-1800 Shimadzu UV spectrophotometer). The rate kinetic change of Langmuir–Hinshelwood reactions depending on time is given below (Eq.)[33];

$$In\mathrm{C}o/\mathrm{C} = \mathrm{kt} \quad \ldots (1)$$

It is calculated with. The slope of the equation is the first order rate constant value (k, min−1).C_0; represents the initial dye concentration and C the dye concentration at time t.

2.3 Photocatalytic activity measurement

To examine the photocatalytic activities of the CeO_2:0.1Dy0.1Ho compound, firstly, 5 ppm methylene blue and malachite green solutions were prepared separately. In each experiment, 10 mg of photocatalyst was suspended in 50 mL of dye aqueous solution. The solution was mixed by keeping it in an ultrasonic bath for a short time. Time-dependent degradation processes of dyestuff molecules were examined between 0 min and 120 min with a 300 W light source. During the examination, 3 mL of solution was removed at regular intervals every 20 minutes. Additionally, the solution was immediately centrifuged and then transferred to a 2 mL quart cuvette and the absorbance spectra were measured. In order to minimize the decrease in volume while taking measurements and to prevent a decrease in the solution volume, the remaining solution from the centrifuge was added back to the solutions under the simulator device. Optical properties of structured particles were measured using a Shimadzu 1800 spectrophotometer.

2.4 Material characterization

TG/DTA analysis was recorded on Seiko Exstar 6000 (Japan) under the nitrogen atmosphere with the heating rate of 10 °C/min and temperature between 30-1000 °C. The X-ray diffraction (XRD: Philips X 'Pert Pro, λ = 0.154056 nm, Cu-Kα radiation)

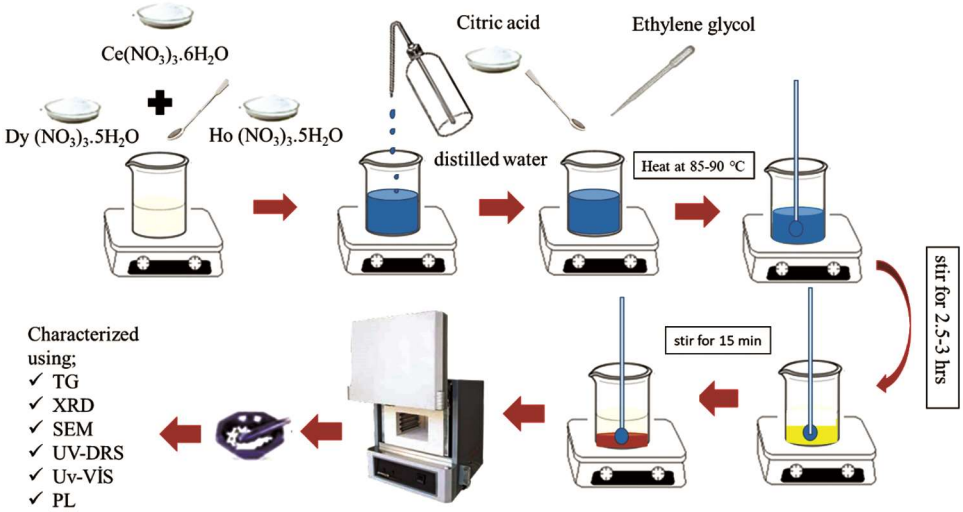

Fig. 1 — Flow chart of sol-gel synthesis of CeO_2:0.1Dy0.1Ho compound.

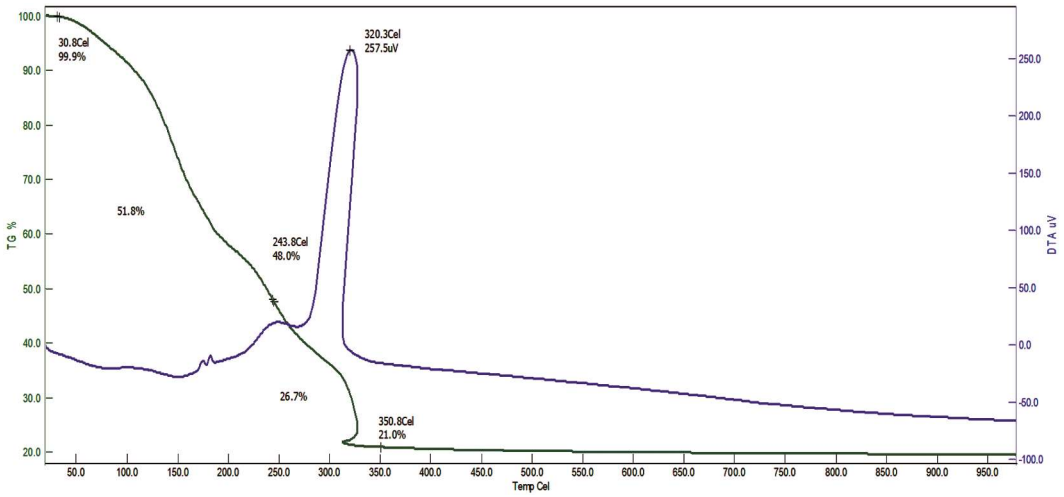

Fig. 2 — Thermal diagram of CeO_2: 0.1Dy0.1Ho compound after pre-drying.

technique was used to reveal the structure of the synthesized compounds. The Raman spectra of the cubic crystal lattice compounds were determined using a portable BWS 465B&W Tek Inc. Raman® spectrometer. The morphological properties of the compounds were examined using a The Zeiss EVO 10 LS scanning electron microscope (SEM). The optical properties of the structured particles were measured using a Shimadzu 1800 spectrophotometer. The Fourier-transform infrared (FT-IR) spectra were recorded using the Perkin Elmer Spectrum 400. Band gap and photocatalytic activity were examined using the Shimadzu 1800 UV–Vis spectrophotometer. The photoluminescence properties were examined with a Fluorescence Spectrophotometer (HITACHI F-7100). All PL measurements were performed with powder samples in an open atmosphere and at room temperature.

3 Result and Discussion

3.1 Thermal Analysis

The TG-DTA graph of the sample taken after the pre-drying process in the sol-gel method is shown in Fig. 2. When the graph is examined, although the mass change was quite high initially, it decreased from 400 °C. The mass change is due to the amount of citric acid, nitrate and molecular water used in the sol-gel method [34]. According to the DTA curve, although there was a phase change at 320 °C, it remained constant thereafter. Cubic crystal lattice formation is after 320 °C. After this temperature, it was determined that the phase remained stable. According to the results of the thermal analysis, the obtained compounds were sintered at 600, 800 and 1000 °C.

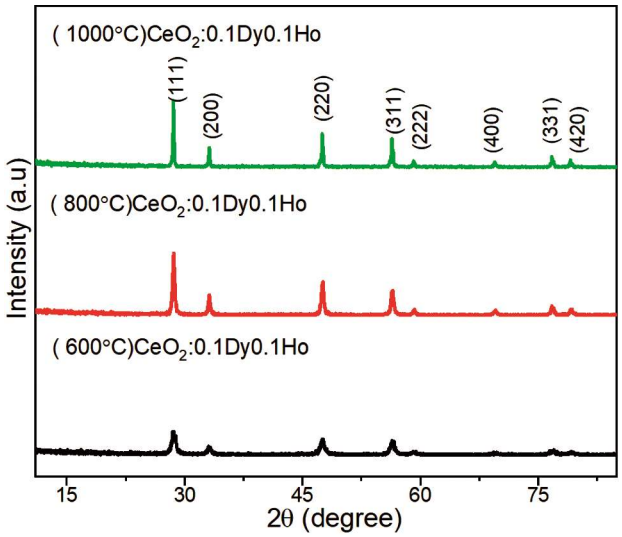

Fig. 3 — X-ray pattern depending on sintering temperature.

3.2 XRD

The x-ray powder diffractometry pattern of CeO_2:0.1Dy0.1Ho compound has been given in Fig. 3. When the patterns were evaluated, it was compatible with the code 98-015-5608. It was determined that the compounds have cubic crystal lattices. As can be seen, after 600 °C, the cubic crystal lattice patterns improved with the increase in temperature. With the increase in temperature, the phase did not decompose and remained stable. The peaks deforming the cubic structure disappeared.

Using the (111)(220)(311) peaks, the crystal parameters were calculated with the Debye-Scherrer formula (Eq. 2). The results were summarized in Table 1.

$$D=k\lambda/\beta\cos\theta \quad \ldots (2)$$

Table 1 — The structure parameters of CeO_2:0.1Dy0.1Ho compound

Samples	Lattice parameters	Volume	Crystalline size (nm)				Micro strain (%)			
	a (Å)	$(Å)^3$	Mean value	(111)	(220)	(311)	Mean value	(111)	(022)	(113)
600°CCeO_2:0.1Dy0.1Ho	5.4051	157.94	11.64	11.51	11.98	11.77	0.83	0.98	0.79	0.69
800°C CeO_2:0.1Dy0.1Ho	5.4079	158.16	16.49	16.99	16.71	15.81	0.74	0.91	0.57	0.52
1000°C CeO_2:0.1Dy0.1Ho	5.4121	158.55	54.83	56.00	50.34	58.82	0.24	0.27	0.12	0.15

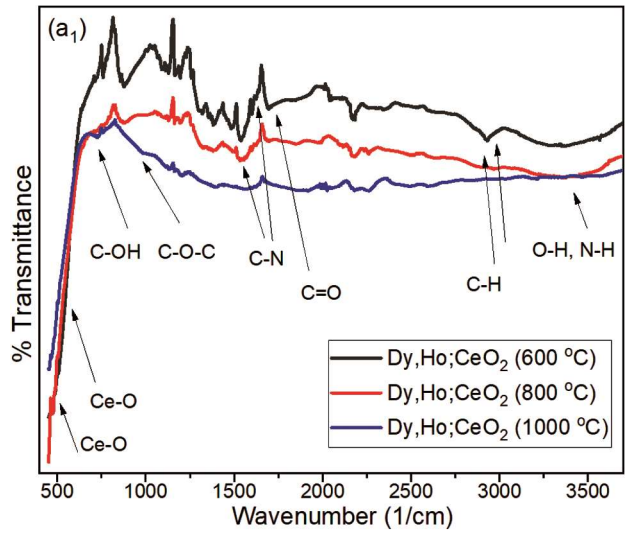

Fig. 4 — Temperature dependent FTIR spectrum of CeO_2:0.1Dy0.1Ho nanostructure.

where k is the Debye-Scherrer constant, λ is the wavelength of the X-ray, β is the FWHM (full width at half maximum) value, and θ is the Bragg diffraction angle.

When Table 1 data is examined, the temperature affects increasing the crystal size. And the synthesized compounds are in the nanostructure.

3.3 Fourier transform infrared spectroscopy (FTIR)

FTIR spectroscopy analysis is used to determine the vibrational motion of atomic/molecular bonds related to different functional groups present on the surface of the synthesized samples with various doping concentrations. Fig. 4 shows the FT-IR spectra of CeO_2:0.1Dy0.1Ho (600-800-1000 °C) in the range of 500 –3750 cm^{-1}. The peak around 500 cm^{-1} is important. Ce–O (M–O) is attributed to the stretching mode and confirms the formation of CeO_2[35]. It was determined that the characteristic absorption bands smoothed as the temperature increased.

3.4 SEM

In Fig. 5, scanning electron microscope images of CeO_2:0.1Dy0.1Ho nanoparticles are presented. Based on these images, grain boundaries have been manually highlighted or automatically detected in representative images, with a varying number of grains ranging from 700 to 1500. Subsequently, the obtained images were analyzed, binarized, and processed using Image J to determine the individual areas of the grains. Upon identification of each grain area, a simple geometric calculation was employed to estimate the approximate grain size using the equivalent area. The grains were assumed to be approximately circular, and thus, the projected grain sizes were estimated from the associated circle diameters. Additionally, particle size diagrams derived from scanning electron microscope images indicate that the sintered compound is in the 110-29 nm rangefrom at different temperatures. When evaluated in conjunction with XRD data, successful attainment of nano-sized compounds is evident in terms of both crystal structure and particle size. Contrary to expectations, particle size decreased as the temperature increased.

3.5 Raman spectroscopy

Raman spectroscopy is a fundamental analysis method to examine the defects in the crystal structure of the synthesized nanostructuredmaterials by doping in the primary phase. Fig. 6 shows the nanostructures Raman peaks of CeO_2:0.1Dy0.1Ho. The fluorite structure of CeO_2 appears to reveal a clear peak at about 464 cm^{-1}, which can be attributed to the F2g mode. This characteristic peak is sensitive to thermal changes, doping, or changes in particle size. In the results of the Raman analysis performed according to the temperature change, although the characteristic peak at 464 cm^{-1} remains constant with the temperature change, the peak intensity changes. In the sample analysis, which was sintered at 1000 °C, peaks were observed at 550 cm^{-1} and 613 cm^{-1}. These peaks indicate the presence of oxygen vacancies in the structure[36].

3.6 Photoluminescence Properties

In the Fig. 7, the excitation spectrum of CeO_2:Dy^{3+}, Ho^{3+} phosphors synthesized at 600, 800 and 1000 °C is shown (λ_{em}:475 nm). In the excitation spectra, a single excitation band at 318 nm was observed and

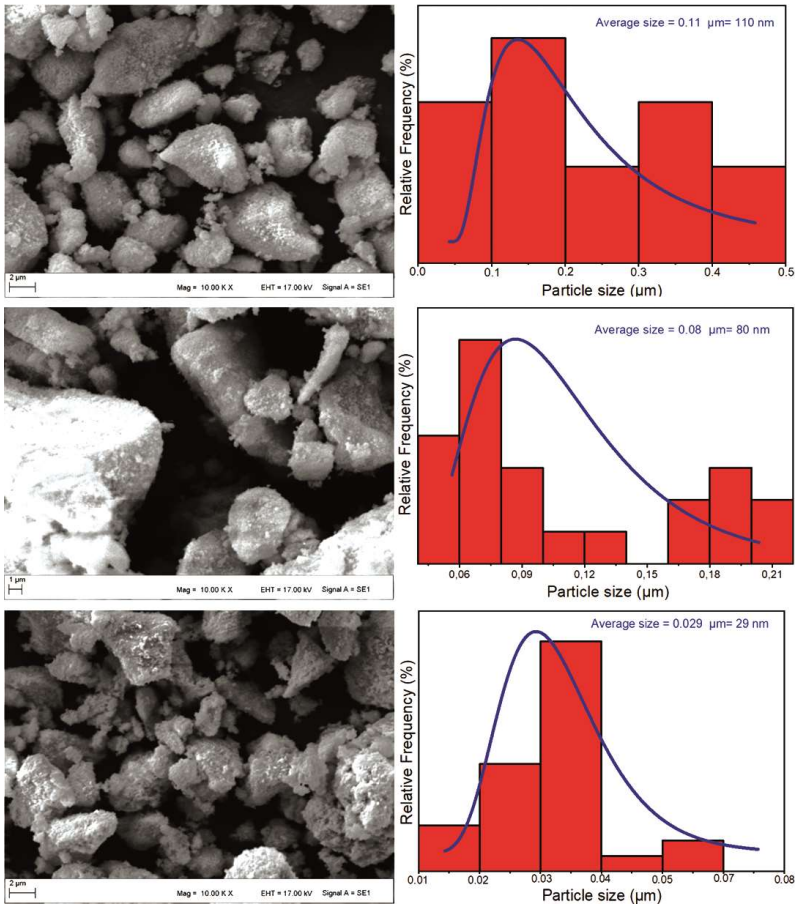

Fig. 5 — Surface images and particle size histogram of CeO_2:0.1Dy0.1Ho nanostructures sintered at 600 °C, 800 °C and 1000 °C.

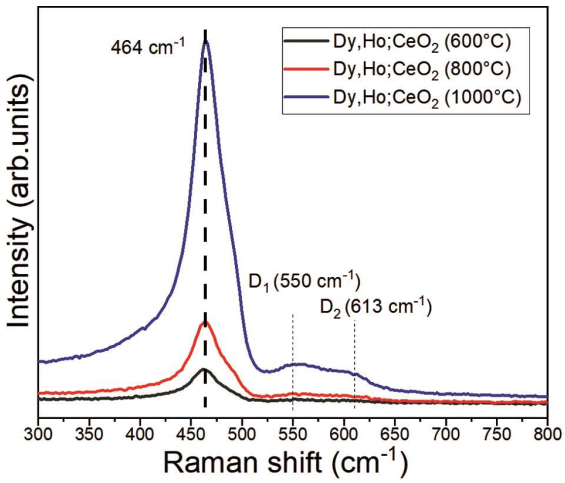

Fig. 6 — Raman spectrum of CeO_2:0.1Dy0.1Ho nanostructures dependent on sintering temperature.

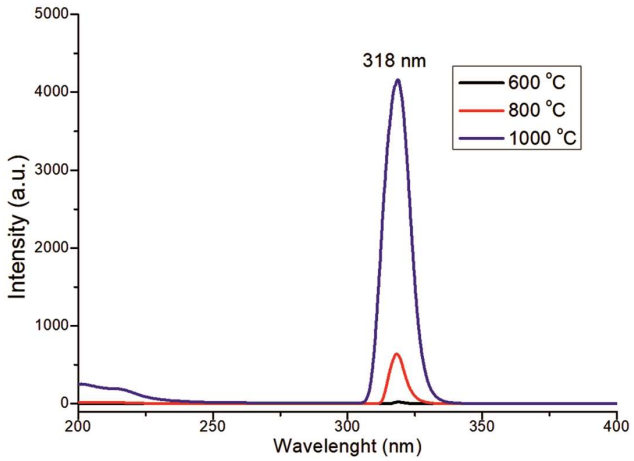

Fig. 7 — The excitation spectra of CeO_2:0.1Dy0.1Ho phosphors synthesized at 600, 800 and 1000 °C.

this excitation band is attributed to $4f^1(^2F_{5/2}) - 4f^05d^1$ transitions of Ce^{3+}ions[37]. It can be seen from Fig. 7 that the excitation band of Dy^{3+} and Ho^{3+} ions are not observed. The intensity of the excitation band increased considerably as the amount of reduced species increased as the reaction temperature increased. In this case, near-UV excited phosphors can be described as host-sensitized luminescent materials. Fig. 8 shows the emission spectrum of CeO_2:Dy^{3+},Ho^{3+} phosphors synthesized at 600, 800 and 1000 °C excited by 318 nm near-UV light. In the

emission spectra, a broad band located from 450 to 700 nm is related to the 5d-4f ($5d^1 \rightarrow 4f^1$) transition of Ce^{3+} ions [38]. Also, there are three maximums at 475 nm (blue), 559 nm (green) and 663 nm (red) on the emission spectrum belonging to Ce^{3+}. It can be seen from the emission spectrum that first dominating emission peak at 475 nm corresponding to $^4F_{9/2} \rightarrow {}^6H_{15/2}$ (blue) transition of Dy^{3+}. The other two emission bands at 559 nm and 663 nm are due to the $^5F_4, {}^5S_2 \rightarrow {}^5I_8$ (green) and $^5F_5 \rightarrow {}^5I_8$ (red) transitions of Ho^{3+} ions, respectively[39]. Just like the excitation intensity, the emission intensity also increases as the reaction temperature increases and the optimum synthesis temperature for CeO_2:Dy^{3+},Ho^{3+} phosphor is 1000 °C. The first reason for the higher luminescence intensity in the CeO_2:Dy^{3+},Ho^{3+} phosphor at 1000 degrees is that the crystal defects that act as luminescence centers increase when the reaction temperature increases. The second reason is as follows: as seen in Figure 3, it is seen that the XRD pattern improves when the reaction temperature increases. Thus, the XRD pattern in Fig. 3 and the structure parameters in Table 1 support the photoluminescence results. Table 1 shows that when the reaction temperature increases, crystalline size increases and micro strain decreases as a result of better crystallization. That is, the increase in luminescence intensity as the temperature increases is a result of better crystallization and the formation of more luminescence centers. When CeO_2:0.1Dy^{3+} 0.1Ho^{3+} phosphor is examined in terms of excitation energy transfer, the excitation energy is captured by the host crystal, and some of the excitation energy is transferred to the activator and co-activator ion, so both the host crystal and the doped ions emit. When photoluminesce emission and excitation spectrum are evaluated together, it is clear that CeO_2:Dy^{3+},Ho^{3+} is excited at near-UV and has blue, green and red emission.

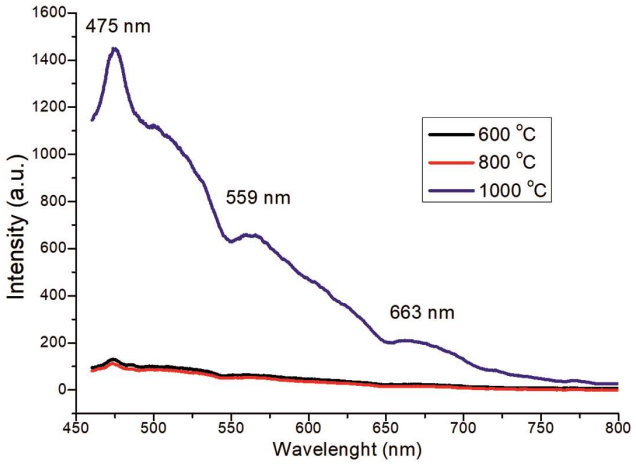

Fig. 8 — The emission spectra of CeO_2:0.1Dy0.1Hophosphors synthesized at 600, 800 and 1000 °C.

3.7 Determination of optical band gap

The modified band structure resulting from changes in nanoscale materials plays a crucial role in determining optical properties. Therefore, a proper understanding of the band structure and the gap between two bands is essential in quantifying nanoscale effects. In this regard, UV-Vis spectroscopy is a widely used standard technique for determining the optical band gap[40].

The optical band gap was estimated from the Touch Plot method obtained using UV-vis spectroscopy and given in Fig. 9. The optical band gap of CeO_2:0.1Dy0.1Ho nanoparticles was determined as 2.43 eV. In the literature, the band gap

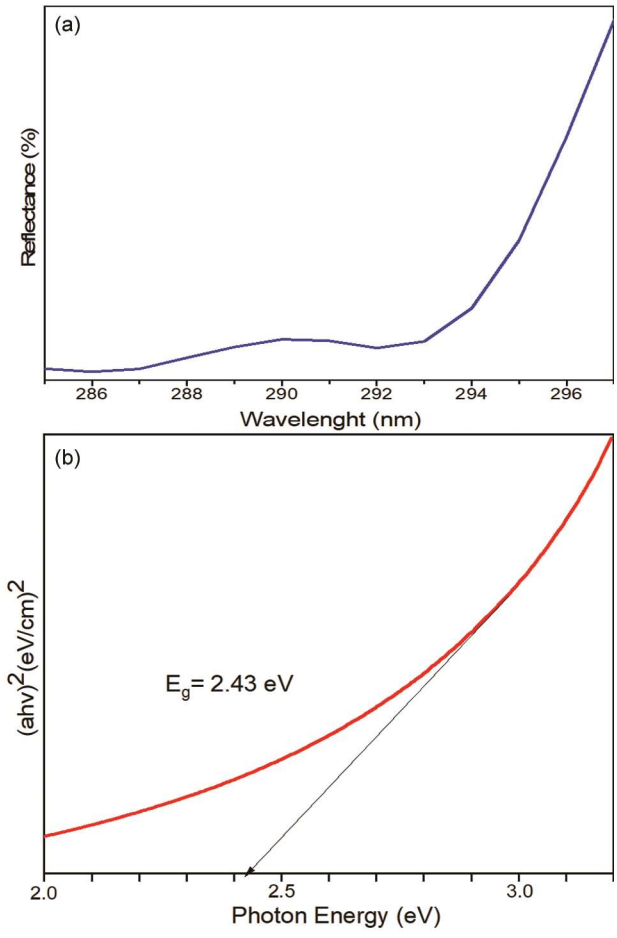

Fig. 9 — Optical band gap of CeO_2:0.1Dy0.1Ho nanostructures and corresponding UV-vis spectrum.

of pure CeO_2 is around 3.2eV[41]. As seen in Fig. 9, in this study, Dy^{3+} and Ho^{3+} ions were doped, and the optical band gap narrowed. This also supported the increase in degradation efficiency.

3.8 UV–vis diffuse reflectance spectral analysis

Methylene blue and malachite green were chosen to investigate the photocatalyst properties of CeO_2:0.1Dy0.1Ho compound. Methylene blue from selected dyestuffs; It is among the dyestuffs frequently used in the pharmaceutical industry, cotton, wood and silk dyeing. It causes prolonged eye burns[42,43]. Malachite green is among the toxic dyestuffs used in the textile industry in wool, yarn, cotton, and back dyeing. It adversely affects the central nervous system and gastrointestinal tract[44]. As it can be understood from their toxic effects, the disposal of both dyestuffs is important. The ability of CeO_2:0.1Dy0.1Ho to be used in the disposal of these dyes has been explained by UV–vis diffuse reflectance spectral analysis.

In the analysis results, the decay absorption graph obtained with time is given in Fig. 10 for methylene blue and Fig. 11 for malachite green. As can be seen, while there is no degradation in the absence of the catalyst, the degradation percentage linearly increased in its presence.

The absorbance data and the dye degradation efficiency were calculated by Eq. 3.

$$\eta=\frac{C0-Ct}{C0}x100 \quad \ldots (3)$$

The values for each sintering temperature are summarized in Table 2. The maximum efficiency for malachite green is 62% at 800 °C, while for methylene blue, it is 90% at 1000 °C.

The obtained CeO_2:0.1Dy0.1Ho nanoparticles offer superior photoactivity for the degradation of organic dyestuffs. As can be seen, the change in temperature positively affects the dyestuff's degradation efficiency. This situation can be explained by the fact that the oxygen vacancy formation in the CeO_2 crystal lattice and the increased superoxide radicals accelerate the dye degradation and increase the efficiency[45].

In our previously published research results, 57% efficiency was found on the methylene blue dye of the compound, which was formed with the (La, Dy) pair and was sintered at 800°C and 1000 °C[46]. In this study, efficiency increase was achieved by doping Dy and Ho.

The following reactions can be predicted during the degradation[47].

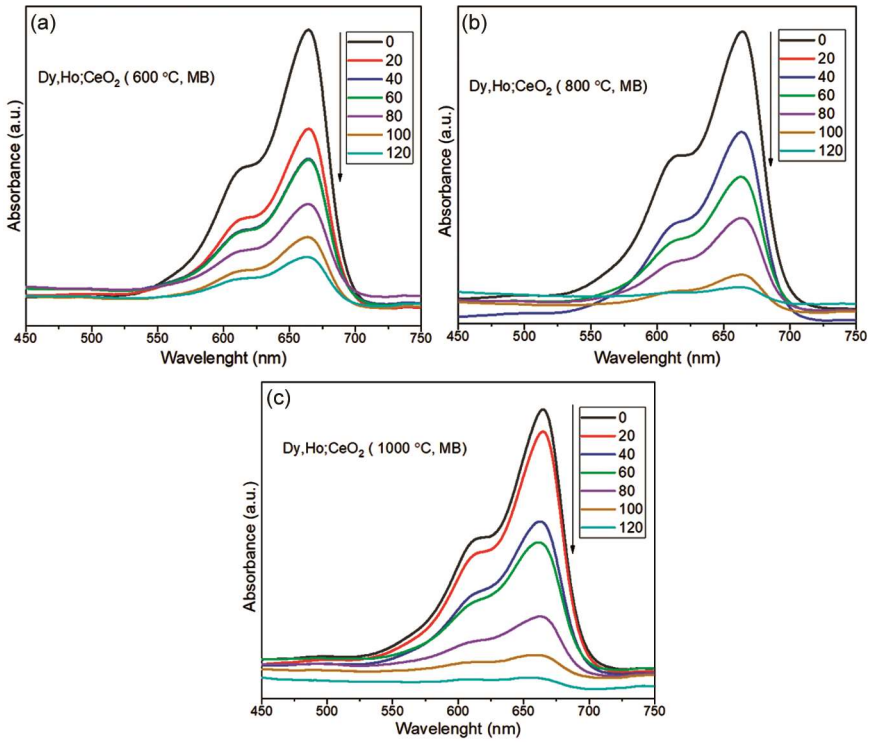

Fig. 10 — Methylene blue absorbance spectra.

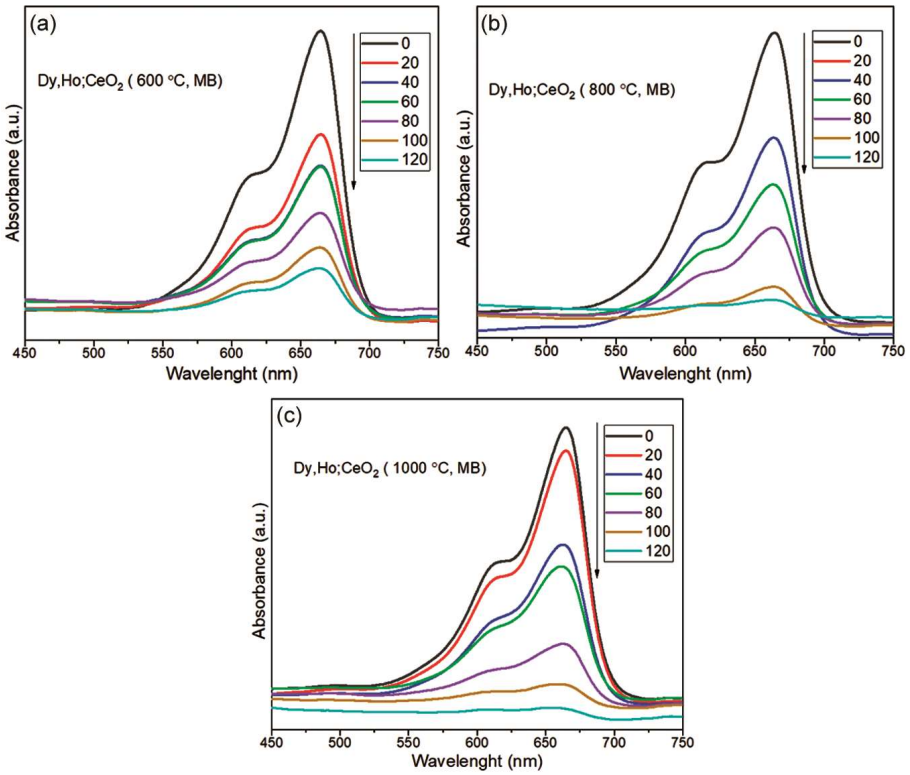

Fig. 11 — Malachite green absorbance spectra.

Table 2 — Variation of degradation efficiency with sintering temperature

Sintering temperature °C	Methylene Blue Degradation efficiency %	Malachite Green Degradation efficiency %
600	71	42
800	84	62
1000	90	33

CeO_2 (Dy, Ho) + *hv* → CeO_2 (Dy,Ho) (e_{CB}^- + h_{VB}^+)

CeO_2 (Dy, Ho) (h_{VB}^+) + H_2O → CeO_2 (Dy, Ho) + H^+ + OH(radical)

CeO_2 (Dy, Ho) (h_{VB}^+) + OH^- → CeO_2 (Dy, Ho) + OH (radical)

CeO_2 (Dy, Ho) (e_{CB}^-) + O_2 → CeO_2 (Dy, Ho) + O_2^-(radical)

O_2^-(radikal) + H^+ → HO_2 (radikal)

dyestuffs+ OH(radical) → degradation product

dyestuffs + h_{VB}^+ → oxidation product

dyestuffs+ e_{CB}^- → reduction product

Fig. 12 shows the Ct/C0 curve graph of 600, 800 and 1000 °C photocatalysts sintered at different temperatures with two different dyestuffs, MB and MG, versus time.

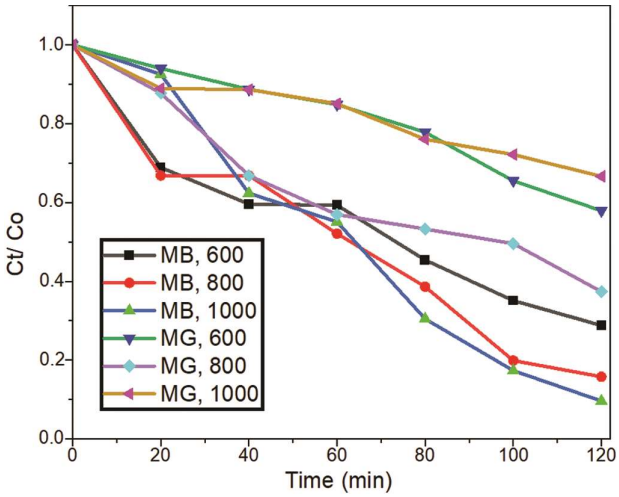

Fig. 12 — Plot of concentration ratio (Ct/Co) versus time.

4 Conclusion

In this paper, the novel near-UV excited CeO_2:0.1Dy0.1Ho phosphor was synthesized by sol-gel method and its photoluminescence and photocatalytic properties were investigated depending on the changing sintering temperature. It was revealed that the applied reaction temperature was a factor that changed the photoluminescence and photocatalytic properties. In this context, the optimum reaction

temperature for CeO_2:0.1Dy0.1Ho phosphor is 1000 1000 °C. While a linear increase in sintering temperature was observed for the degradation of methylene blue in photocatalytic performance, the optimum for malachite green was found to be 800 °C. These results allow understanding the synergistic effect of rare earth elements used as additives in enhancing the photocatalytic properties of the host crystal and provide important information for the design and optimization of photocatalysts for advanced applications. Additionally, the host-sensitized CeO_2:0.1Dy0.1Ho phosphor synthesized at 1000 °C has blue, green and red emission bands and exhibits very good photoluminescence properties for w-LEDs and optoelectronic applications.

References

1 Li Y, Lin J, Xie B & Liu G, *J Wuhan Univ Technol-Mater Sci Ed*, 35 (2020) 335.
2 Korotcenkov G, *Elsevier*, (2019)
3 Grinter D C & Thornton G, *J Phys: Cond Matter*, (2022).
4 Bui H T, Weon S, Bae J W, Kim E J, Kim B, Ahn Y Y & Kim W, *J Hazard Mater*, 404 (2021) 123976.
5 Bakir A H & Torun H Ö, *J Chem Soc Pak*, 43 (2021).
6 Ozlu T H & Çakar S, *J Therm Anal Calor*, 133 (2018) 1233.
7 Basavaraj R B, Navami D, Deepthi N H, Venkataravanappa M, Lokesh R, Kumar K S & Sreelakshmi T K, *Inorg Chem Commun*, 120 (2020) 108164.
8 Pal A K, Som S & Lu C H, *Ceram Int*, 44 (2018) 18256.
9 Mohanty B & Nayak J, *Mater Res Exp*, 4 (2017) 115015.
10 Gnanam S, Gajendiran J, Ramya J R, Ramachandran K & Raj S G, *Chem Phys Lett*, 763 (2021) 138217.
11 Raj A K, Rao P P, Sreena T S & Thara T A, *Phys Chem Chem Phys*, 19 (2017) 20110.
12 Malleshappa J, Nagabhushana H, Sharma S C, Sunitha D V, Dhananjaya N, Shivakumara C & Nagabhushana B M, *J Alloys Compd*, 590 (2014) 131.
13 Singh V, Rathaiah M, Venkatramu V, Haase M & Kim S H, *Spectrochim Acta Part A: Mol Biomol Spectr*, *122*(2014)704-710.
14 Oikawa M & Fujihara S, *J Eur Ceram Soc*, 25 (2005) 2921.
15 Kırkgeçit R, Torun H Ö, Dokan F K & Öztürk E, *J Rare Earths*, 40 (2022) 1619.
16 Jasim S A, Machek P, Abdelbasset W K, Jarosova M, Majdi H S & Khalaji A D, *Appl Phys A*, 128 (2022) 1.
17 Akbari-Fakhrabadi A, Saravanan R, Jamshidijam M, Mangalaraja R V & Gracia M A, *J Saud Chem Soc*, 19 (2015) 505.
18 Xu B, Yang H, Zhang Q, Yuan S, Xie A, Zhang M & Ohno T, *Chem Cat Chem*, 12 (2020) 2638.
19 Kırkgeçit R, Torun H Ö, Dokan F K & Öztürk E, *J Photochem Photobiol A: Chem*, 423 (2022) 113602.
20 Xia X, Li J, Chen C, Lan Y P, Mao X & Bai F, *Nanotechnology*, 32 (2021) 195708.
21 Öztürk E & Ozpozan Kalaycioglu N, *J Therm Anal Calorimet,* 117 (2014) 573.
22 Öztürk E & Sarılmaz E, *Mater Chem Phys,* 239 (2020) 122085.
23 Öztürk E & Sarılmaz E, *Mater Res Exp*, 6 (2019) 105710.
24 Liu Y, Yang Z, Yu Q, Li X, Yang Y & Li P, *Mater Lett,* 65 (2011) 1956.
25 Uzun E, Öztürk E & Ozpozan K N, *Luminescence,* 33 (2018) 1346.
26 Öztürk E, Kalaycioglu N O & Uzun E, *J Chin Chem Soc*, 62 (2015) 47.
27 Zhang R & Wang X, *J Alloys Compd*, 509 (2011) 1197.
28 Shinde K N, Dhoble S J & Kumar A, *Phys B: Cond Matter*, 406 (2011) 94.
29 Do H S, Khatkar S P, Taxak V B, Sharma G & Kumar D, *Mater Sci Eng B*, 129 (2006) 126.
30 Xiao Y, Jin X, Zhang L, Luo H & Li J, *Integr Ferroelect*, 191 (2018) 169.
31 Kunimi S & Fujihara S, *ECS J Solid State Sci Technol*, 1 (2012) R32.
32 Rajesh K, Sakthivel P, Santhanam A & Venugobal J, *Optik*, 216 (2020) 164800.
33 Kirkgecit N, Kirkgecit R, Torun H Ö, Urus S & Bozgeyik M S, *J Mater Electron Dev*, 5 (2023) 21.
34 Kirkgeçit R & Torun H Ö, *Process Appl Ceram*, 14 (2020) 314.
35 Khadar Y S, Balamurugan A, Devarajan V P & Subramanian R, *Orient J Chem*, 33 (2017) 2405.
36 El-Habib A, Addou M, Aouni A, Diani M, Zimou J, Bouachri M & Jbilou M, *Mater Sci Semicond Process*, 145 (2022) 106631.
37 Li X, Liu H, Wang J, Cui H & Han F A G, *Mater Res Bull*, 39 (2004) 1923.
38 Lu F C, Guo S Q, Yang Z P, Yang Y M, Li P L, Li X & Liu Q L, *J Alloys Compd*, 521 (2012) 77.
39 Linqing S, Yan Z, Xusheng W & Yanxia L, *Mater Res Bull*, 144 (2021) 111495.
40 Sonkar R, Mondal N J, Boro B, Ghosh M P & Chowdhury D, *J Phys Chem Sol*, 185 (2024) 111715.
41 Orel ZC & Orel B, *Physica Status Solidi (B)*, 186 (1994) 33.
42 Jack C I I, & Leikin, J B, *Am J Therap*, 10 (2003) 289.
43 Rafatullah M, Sulaiman O, Hashim R & Ahmad A, *J Hazard Mater*, 177 (2010) 70.
44 Mittal A, *J Hazard Mater*, 133 (2006) 196.
45 Yang H, Xu B, Yuan S, Zhang Q, Zhang M & Ohno T, *Appl Catal B: Environ*, 243 (2019) 513.
46 Torun H Ö, Kırkgeçit R, Dokan F K & Öztürk E, *J Photochem Photobiol A: Chem*, 418 (2021) 113338.
47 Ma R, Zhang S, Wen T, Gu P, Li L, Zhao G & Wang X, *Catal Today*, 335 (2019) 20.